Batteries & Supercaps

Research Article
doi.org/10.1002/batt.202200336

Chemistry Europe
European Chemical Societies Publishing

www.batteries-supercaps.org

Special Collection

Reactivity of TiS_2 Anode towards Electrolytes in Aqueous Lithium-Ion Batteries

Leiting Zhang,[a] Xu Hou,*[a] Kristina Edström,[a] and Erik J. Berg*[a]

Aqueous rechargeable batteries are appealing alternatives for large-scale energy storage. Reversible cycling of high-energy aqueous batteries has been showcased using highly concentrated aqueous electrolytes, which lead to a significantly suppressed water activity and formation of a stable solid-electrolyte interphase (SEI). However, the high salt concentration inevitably raises the cost and compromises the environmental sustainability. Herein, we use layered TiS_2 as a model anode to explore the feasibility of cycling aqueous cells in dilute electrolytes. By coupling three-electrode cycling data with online electrochemical mass spectrometry measurements, we depict the potential-dependent gas evolution from the cell in the absence of a stable SEI. We offer a comprehensive mechanistic understanding of the complex interfacial chemistry in dilute electrolytes, taking into account material reactivity and interfacial compatibility. Design strategies and research directions of layered-type electrodes for sustainable aqueous batteries with dilute electrolytes are recommended, based on the scientific discovery presented in this work.

Introduction

Rechargeable batteries are accelerating the transition from fossil fuels to renewable energies. Considering the enormous amounts of battery materials needed, sustainability in materials and processes is of the highest importance. Among various next-generation battery chemistries, aqueous lithium-ion batteries (ALiBs) stand out for being intrinsically safe, even at high power densities, and can likely be implemented in existing established production processes of Li-ion cells based on non-aqueous electrolytes. For instance, as first proposed by Li et al.,[1] ALiBs are sustainable alternatives to conventional batteries containing organic solvents, as water-based electrolytes are environmentally friendly, non-flammable, and inexpensive. While ethical concerns and environmental impacts of lithium mining need to be seriously addressed, the considerably higher ionic conductivity of aqueous electrolytes offers much more appealing fast-charging capabilities for ALiBs. However, its wide implementation has been significantly hindered by water's narrow electrochemical stability window (ESW) of 1.23 V, beyond which water electrolysis will take place, leading to hydrogen evolution reaction (HER) and oxygen evolution reaction (OER). In comparison, traditional non-aqueous Li-ion batteries possess a wide ESW of ~3 V, which can be further enlarged by the formation of a so-called solid-electrolyte interphase (SEI).[2] The SEI formation is largely due to the electrochemical decomposition of the organic electrolyte solvents outside their ESWs and the precipitation of insoluble degradation products on the electrode surface. Unfortunately, typical inorganic ion-conducting salts used for ALiBs, such as sulfates, nitrates, and perchlorates, are insufficiently surface-active to form the much-needed SEI, hence the continuous water decomposition when the anode potential is lower than the hydrogen evolution potential.

The development of ALiBs gradually fell into obsolescence until 2015, when Suo *et al.* reported the use of a highly concentrated electrolyte, consisting of 21 mol kg^{-1} (molality, m) of lithium bis(trifluoromethane sulfonyl)imide (LiTFSI) in water, also known as the "water-in-salt" (WiS) electrolyte.[3] Under such a high salt concentration, water activity is suppressed and its ESW significantly enlarged. An SEI composed mainly of LiF, from the decomposition of $TFSI^-$ anions, enables an extremely wide ESW of ~3 V despite the presence of water. The same strategy has been pursued with the emergent novel electrolyte discoveries, such as hydrate-melts and aqueous deep eutectic solvents,[4–6] in which the ultimate goal has been to reduce the reactivity of free water in the electrolyte. Although scientifically fascinating, the high cost and low environmental sustainability associated with the high salt concentrations in WiS electrolytes impede their successful commercialization.[7] In this regard, it is appealing to bring aqueous electrolytes back to the "salt-in-water" regime and search for alternative SEI formers, *e.g.*, based on molecular agents (CO_2) or using molecular-crowding electrolytes.[8,9]

Meanwhile, the proper selection of electrode materials is of vital importance for the successful operation of ALiBs. While spinel $LiMn_2O_4$ is often the "go-to" choice for ALiBs, owing to its optimal potential window and commercial availability, there

[a] Dr. L. Zhang, Dr. X. Hou, Prof. K. Edström, Prof. E. J. Berg
Department of Chemistry – Ångström Laboratory
Uppsala University
P.O. Box 538, SE-751 21 Uppsala, Sweden
E-mail: xu.hou@kemi.uu.se
erik.berg@kemi.uu.se

Supporting information for this article is available on the WWW under https://doi.org/10.1002/batt.202200336

Special Collection *An invited contribution to a Special Collection dedicated to Aqueous Electrolyte Batteries*

Research Article
doi.org/10.1002/batt.202200336
Chemistry Europe
European Chemical Societies Publishing

is a plethora of anode materials proposed in literature, such as Mo_6S_8, TiS_2, TiO_2, $Li_4Ti_5O_{12}$, $LiTi_2(PO_4)_3$, *etc.*[10] Screening through the list, titanium disulfide (TiS_2) stands out for being commercially available at scale and the lightest weight and lowest cost dichalcogenide with historical application in batteries. Indeed, TiS_2 was employed in the first rechargeable Li battery conceived by Nobel laureate Stanley Whittingham in the 1970s.[11,12] Since then, TiS_2 has been documented as a versatile host to accommodate different types of intercalants (H^+, Li^+, Na^+, K^+, NH_4^+, Mg^{2+}, Zn^{2+}, Ca^{2+}).[13–20] However, TiS_2 and other similar transition metal dichalcogenides (MoS_2, *etc.*) have also been widely exploited for electrocatalysis purposes to accelerate HER, hence lowering its suitability as battery anode.[21,22] Sulfur vacancy defects in these transition metal dichalcogenides may function as active sites for HER with low overpotential, resulting from the low adsorption free energy of H atoms.[21] In addition, since the adjacent S–Ti–S layers are weakly linked by the van der Waals interactions, catalytically active single-layered TiS_2 sheets are typically prepared following an intercalation-exfoliation route, which involves partially lithiated Li_xTiS_2 as a precursor.[23] Moreover, the compatibility of TiS_2 with water may be questioned, as the oxygen atom from water may interact and replace the edge sulfur atom, following $TiS_2 + xH_2O \rightarrow TiS_{2-x}O_x + xH_2S$.[24] Nevertheless, TiS_2 has recently been proposed by Sun *et al.* as a viable anode for ALiBs,[25] but the nature and extent of its reactivity towards aqueous battery electrolytes remain largely unclear.[26]

In order to address the issue, we herein present an exploratory study on the feasibility of cycling TiS_2 against $LiMn_2O_4$ in a comparatively dilute (2 m) aqueous electrolyte. The electrode potential, measured *via* a three-electrode cell, is coupled with online electrochemical mass spectrometry (OEMS) to analyze eventual TiS_2/electrolyte interfacial side-products. Using TiS_2 as a model anode, we aim to provide further fundamental insights of electrode-electrolyte interactions in ALiBs, which can be generalized to other electrochemical systems alike.

Results and Discussion

Electrochemical performance

The electrochemical performance of TiS_2 was first assessed in coin-type aqueous Li-ion full-cells. The galvanostatic dis-/charge profile of a typical cell is plotted in Figure 1. To avoid confusion, charge is defined always with respect to the full-cell, *i.e.*, $LiMn_2O_4$ delithiation and TiS_2 lithiation. When cycled against an oversized $LiMn_2O_4$ cathode using a dilute electrolyte (2 m LiTFSI in H_2O), the cells deliver a reversible discharge capacity around 80 mAh g^{-1} between 0.01–1.8 V at 0.2 C (1 C = 250 mA g^{-1}) in the first five cycles. In contrast, a gradual flattening of the end-of-charge profile (red-shading in Figure 1) strongly suggests increasing extents of water reduction. Given that the corresponding discharge capacity does not change over the first five cycles, the increasing charge capacity is most likely caused by the high HER activity in the dilute electrolyte,

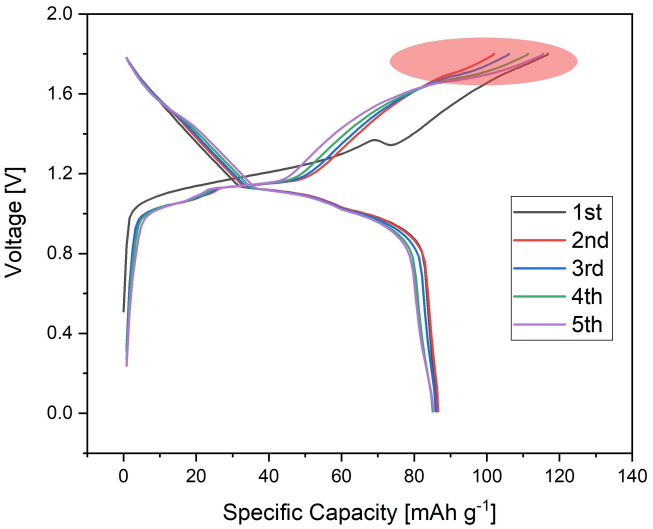

Figure 1. Galvanostatic cycling profiles of $LiMn_2O_4||TiS_2$ cycled in 2 m LiTFSI aqueous electrolyte. The red-shaded region is associated with increasing water reduction.

in the absence of a stable SEI. The Coulombic efficiency (CE) continuously drops upon cycling from 88% in the 3rd cycle to 70% in the 20th cycle in a representative full-cell, as illustrated in Figure S1 in the supporting information. In comparison, effectively suppressed water reduction was reported by Sun et al., in which the same chemistry ($LiMn_2O_4||TiS_2$) was successfully cycled in a 21 m LiTFSI WiS electrolyte over 50 cycles at 1 C.[25] It is however worth noting that in the study, the authors attempted to charge the full-cell to 2.3 V in dilute electrolytes (either 1 m $LiNO_3$ or 1 m LiTFSI) but failed. To make a direct comparison, we also cycled $LiMn_2O_4||TiS_2$ full-cells using 1 m LiTFSI electrolyte with 2.3 V upper cutoff voltage. Decent electrochemical performance was obtained before the voltage reaching ca. 2.0 V (Figure S2). Afterwards, the profile started to flatten, indicative of more pronounced HER, until reaching the preset cut-off time limit. Therefore, the improved cycling stability at low salt concentrations in this study is to a less extent related to the applied voltage window, but can be most likely attributed to a more corrosion-resistive cell configuration-all metallic parts of the cells used in this study (three-electrode cell, OEMS cell) are made of 316 L-type stainless steel. In addition, the quality of TiS_2 used in this study may differ from the one in the referenced work, which may also be a source of discrepancy.

Besides the unexpected cycling performance, the peculiar potential profile of the full-cell also caught our attention. Recall that TiS_2 is a classical Li-ion battery anode with a documented redox potential centered around 2.2 V vs. Li^+/Li^0 (the electrode potential will hereafter always be referred to metallic Li, if not otherwise specified).[12] Knowing that the potential of the oversized $LiMn_2O_4$ cathode should stay around 4.0 V, the potential of the TiS_2 electrode, as deduced from the full-cell voltage, is unexpectedly high. To clarify that, we constructed a Swagelok-type three-electrode cell, by incorporating a commercial Ag/AgCl reference electrode to individually depict the

Research Article
doi.org/10.1002/batt.202200336
Chemistry Europe
European Chemical Societies Publishing

anode and cathode potentials. A TiS_2 half-cell against metallic Li was also assembled, using a classical non-aqueous electrolyte (1 mol L^{-1} $LiPF_6$ in a mixture of ethylene carbonate-diethyl carbonate, 1:1 by weight, also known as the LP40 electrolyte). Figure 2 compares the fifth-cycle potential profile of TiS_2 cycled in both aqueous and non-aqueous electrolytes. The reconstructed electrode potentials of the aqueous full-cell and the TiS_2 potential in the non-aqueous half-cell are presented in Figure S3 and Figure S4, respectively.

The potential profile of TiS_2 in the aqueous electrolyte possesses distinctly different features compared to the one obtained in non-aqueous electrolytes. Two plateaus centered around 2.95 V and 2.88 V are observed, followed by a tail with a much steeper slope between 2.3–2.8 V. Note that the potential profile of TiS_2 upon further charge between 2.3–2.5 V slightly flattens, as compared to the region between 2.5–2.8 V, which can be ascribed to accelerated water reduction. On the other hand, TiS_2 cycled in the LP40 electrolyte shows a characteristic potential profile centered around 2.2 V. We attempted to positively polarize the potential above 3 V upon discharge, but did not observe any additional plateaus similar to those found in the aqueous cell.

Such a discrepancy challenges our perception of the cycling mechanism of TiS_2 in aqueous batteries. Even in the very first cycle, before any water decomposition could take place, the potential profile of TiS_2 is drastically different from the non-aqueous one. Since Sun et al. also observed a similar potential profile using a 21 m WiS electrolyte, it is reasonable to speculate that solvated water and/or hydronium cation (H_3O^+) participates in the intercalation reaction and alters the electrode potential. Indeed, hydronium cations can be intercalated into electrode materials, as in the previously reported hydronium-ion batteries.[13] The presence of H_3O^+ during open-circuit voltage was confirmed by a prompt pH measurement, showing a slightly acidic solution with a pH of 5.3. In fact, a similar potential profile is anticipated from the work of Li et al., who possibly already demonstrated proton intercalation into TiS_2 and $Na_{0.14}TiS_2$ in an acidic aqueous Zn-ion electrolyte.[27] Their reported potential profiles (Figure S3 in their Supplementary Information) are similar to ours (Figure 2 above) on the same potential scale with qualitatively resembling features, i.e., plateaus around 2.9 V followed by a steeper tail. Most importantly however, our cells display much better cycling performance with higher capacities, which may originate from 1) enhanced electrolyte kinetics, 2) presence of Li^+ in the electrolyte, and/or 3) higher quality TiS_2 used.

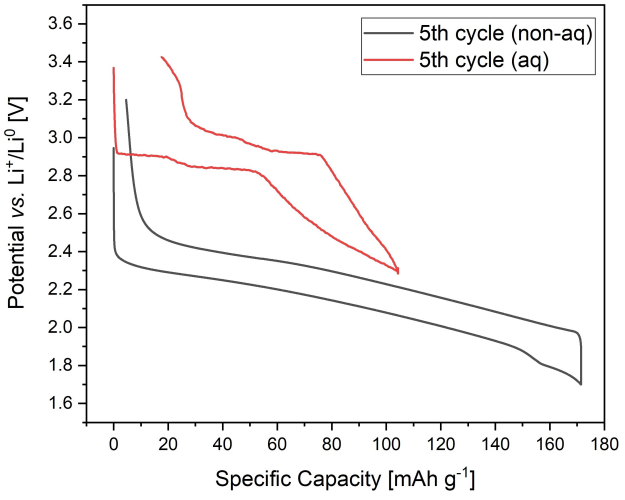

Figure 2. Comparison of representative potential profiles of TiS_2 cycled in a non-aqueous electrolyte (black) and that cycled in an aqueous electrolyte (red).

Operando gas analysis

Since water decomposition is typically accompanied by gas evolution, OEMS is highly suitable to study aqueous chemistries. The technique qualitatively and quantitatively analyzes the volatile species formed inside the cell in real time, which has proven extremely relevant in depicting interfacial reactions in various battery chemistries (Li-ion, Na-ion, solid-state, Li–O_2, aqueous, *etc.*).[9,28–33] Moreover, the onsets of gas evolution can be linked to the electrode potential in parallel, owing to the advantage of running three-electrode measurement in a Swagelok-type cell. This combination is of vital importance for aqueous battery studies, since the HER and OER are intrinsically determined by the electrode potentials.

Figure 3 systematically compares the synchronized electrode potentials and gas evolution rates as functions of the cycling time. The $m/z = 2$, 34, and 64 channels are assigned to H_2, H_2S, and possibly volatile elemental sulfur (S_8), respectively. The $m/z = 32$ channel was also recorded to monitor O_2, but no evidence of O_2 evolution was observed and the channel rather turned out to be fully overtaken by the signal of H_2S. Also note that only H_2 has been calibrated, whereas H_2S and S_8 are only qualitatively estimated.

H_2 evolution is consistently observed at high cell polarizations as a result of HER at the anode. Interestingly, the HER onset potential rises from *ca.* 2.68 V in the first cycle to ca. 2.80 V in three cycles and stabilizes thereafter. According to the Nernst equation, $E_{HER} = -0.059$ pH, an increased hydrogen evolution onset potential implies a decreased electrolyte pH. In other words, the dilute aqueous electrolyte has been notably acidified. A back-of-the-envelope calculation suggests the electrolyte pH should drop from 5.4 to 3.4 upon cycling the TiS_2 electrode, which agrees with the values measured *ex situ*. Although one should be cautious to define the "pH" of a 2 m electrolyte, the values would qualitatively reflect the change of the associated proton activity.

Furthermore, the maximum H_2 release rate r_{max} and the absolute amount of H_2 evolved in each cycle n_{abs} are quantified in Table 1. While r_{max} gradually stabilizes, n_{abs} increases almost linearly in the first five cycles. Such a discrepancy, which has been identified from a previous OEMS study,[34] is ascribed to a longer time the anode spent at low potentials in the succeeding cycles.

Potential-dependent formation of H_2S gas is observed by OEMS. The detection of the noxious H_2S gas does not come as

Research Article
doi.org/10.1002/batt.202200336
Chemistry Europe
European Chemical Societies Publishing

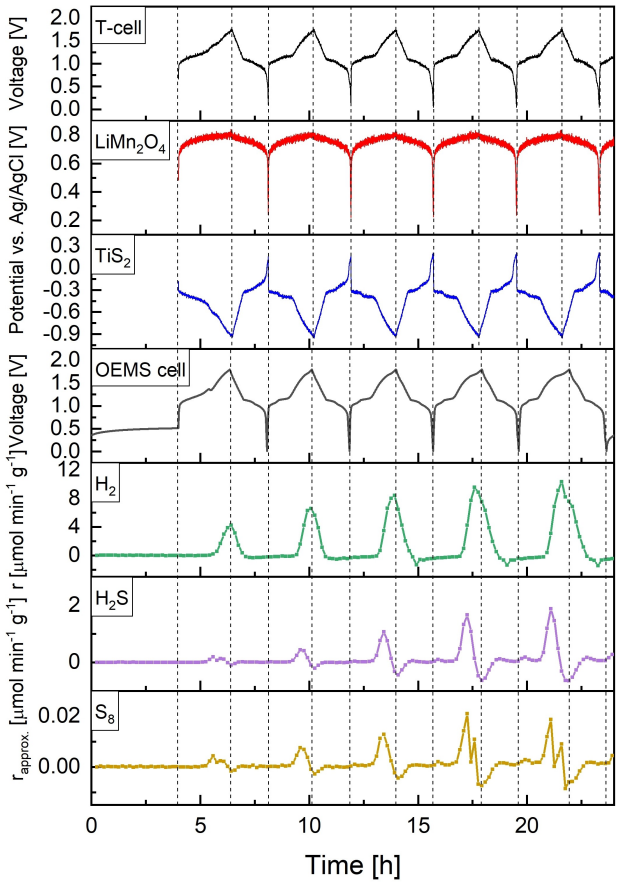

Figure 3. *Operando* gas analysis coupled with three-electrode measurements to show potential-dependent formation of gases in a $LiMn_2O_4$||TiS_2 full-cell. The three-electrode measurement was performed in a T-shaped Swagelok cell using a commercial Ag/AgCl reference electrode, while ion currents corresponding to gases and volatile species were recorded from a home-made OEMS cell.

Table 1. Quantitative assessment of H_2 Evolution.

	Cycle 1	Cycle 2	Cycle 3	Cycle 4	Cycle 5
Onset potential on TiS_2 [V]	2.68	2.77	2.80	2.80	2.80
r_{max} [nmol min^{-1}]	19.77	30.77	39.41	44.77	48.38
n_{abs} [µmol]	0.94	1.48	1.95	2.50	2.96

a surprise, as a rotten egg smell is often recognized when disassembling TiS_2-containing cells. H_2S starts to evolve at the end of the 1.19 V plateau of the full-cell upon charge, or 2.80 V of the TiS_2 electrode detected by the three-electrode cell. While the onset of H_2S is slightly earlier than that of H_2, its maximum evolution rate in each cycle coincides with the fastest increase of H_2 evolution rate, indicating a strong correlation between the two. This is also supported by the negative formation rates, *i.e.*, consumption of H_2S, when the H_2 evolution is taking place. We further confirm the correlation by charging an OEMS full-cell to only 1.2 V, before reaching the onset of H_2S release, and no H_2 is detected (Figure S5).

Signal at $m/z=64$ is repeatedly detected and follows roughly the H_2S evolution profile. An educated guess for the signal, based on the $LiMn_2O_4$||TiS_2 chemistry cycled in the 2 m LiTFSI electrolyte, would be elemental sulfur, a partial oxidation product of H_2S.[35] It is worth mentioning that sulfur dioxide (SO_2) also has the m/z fraction at 64, but it is formed when H_2S is completely oxidized in an O_2-rich environment,[36] which is not the case here. To exclude the contribution from the electrolyte salt $LiN(SO_2CF_3)_2$ that also contains nominal "SO_2" groups, an OEMS cell was constructed, using a 2 m $LiClO_4$ aqueous electrolyte. As shown in Figure S6, similar cycling performance and gas release behaviors are noted, including the repeated signal at $m/z=64$. Therefore, the signal can be unambiguously assigned to elemental sulfur. The peak-splitting in the following cycles has been observed in multiple cells, therefore, it should correlate with a different oxidative process. However, given the trace amount of S_8, its impact to overall cycling performance remains low.

Interestingly, a minor voltage bump is observed in the first charge at ca. 1.4 V, which is often interpreted as a nucleation/growth process[37] or a dissolution/precipitation process.[38,39] After resting a full-cell at OCV for 12 h (Figure S7), the mild bump can still be observed, which occurs when the accelerated H_2 evolution sets in. Therefore, the bump in the first cycle is likely associated with accelerated proton reduction, while the H_2S evolution is electrochemically triggered (*i.e.*, voltage sensitive) but chemically formed, as a result of trace TiS_2 dissolution.

Reaction schematic

Having discussed individual formation pathways for H_2, H_2S, and elemental sulfur, we propose a reaction scheme to account for the peculiar potential profile of TiS_2 and the evolution of all volatile species along cycling, by considering material properties of TiS_2 and respective causalities (Scheme 1).

TiS_2 may react with H_2O in the electrolyte during OCV. The reaction may start from TiS_2 prismatic edge planes, but with a limited rate.[24] The early intercalation reaction expands the *c*-axis and allows more H_2O to diffuse into the interlayer, which

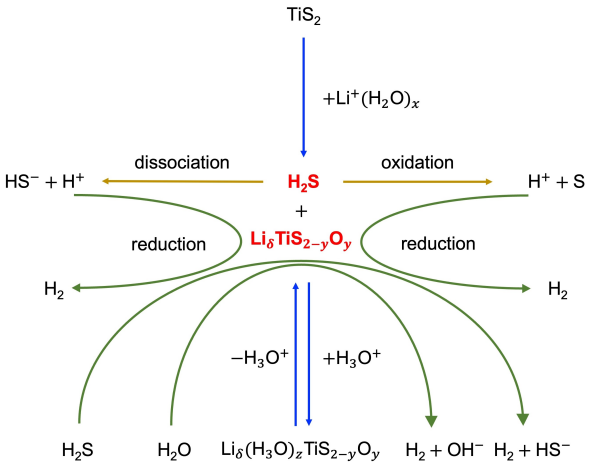

Scheme 1. Evolution of TiS_2 in a dilute aqueous electrolyte upon cycling.

will significantly accelerate the O–S exchange, hence the release of H_2S.

$$TiS_2 + Li^+(H_2O)_x + e^- \rightarrow Li_\delta TiS_{2-y}O_y + H_2S \quad (1)$$

The as-formed H_2S has a pK_a of 7.05 and is slightly soluble in water. Its dissociation may acidify the electrolyte.

$$H_2S \rightarrow HS^- + H^+ \quad (2)$$

Part of the dissolved H_2S may diffuse to the positive electrode and be oxidized at a potential of *ca.* 4.0 V to form elemental sulfur and proton.[40] The proton may in turn acidify the electrolyte.

$$H_2S \rightarrow S + 2H^+ + 2e^- \quad (3)$$

Upon further charge, excess hydronium cations may be attracted to the TiS_2 electrode. Part of them will intercalate into the expanded layered structure of TiS_2, which acts as a reversible hydronium-ion battery anode.

$$Li_\delta TiS_{2-y}O_y + zH_3O^+ + ze^- \leftrightarrow Li_\delta(H_3O)_zTiS_{2-y}O_y \quad (4)$$

The repeated expansion-contraction of the lattice and O–S exchange will inevitably deteriorate the structural integrity of the layered TiS_2 structure, leading to partial exfoliation and defective S-vacancy formation.[22,26] New interfaces will form, providing extra active sites to catalyze HER at low potentials. When the electrolyte is acidic, protons/hydronium cations will be reduced into H_2, while in neutral and basic electrolyte solutions, H_2O will be reduced into H_2 and OH^-. In addition, at the current time we cannot fully exclude the direct electrochemical reduction of H_2S, which should proceed in a similar way as in H_2O reduction.

$$2H^+ + 2e^- \rightarrow H_2 \quad (5)$$

$$2H_2O + 2e^- \rightarrow H_2 + 2OH^- \quad (6)$$

$$2H_2S + 2e^- \rightarrow H_2 + 2HS^- \quad (7)$$

Discussion

Given the complex chemical and electrochemical reactions listed in Scheme 1, the feasibility of using TiS_2 as a practical anode for ALiBs based on dilute electrolytes remains questionable. On the one hand, we demonstrate that TiS_2 can be cycled in dilute (2 m) aqueous electrolytes with a decent initial discharge capacity of ca. 80 mAh g^{-1}. On the other hand, the Coulombic efficiency of all the cells remains below 90% and continues deteriorating, suggesting severe side-reactions (HER, structural degradation, *etc.*) in the absence of a stable SEI. This is further supported by a self-discharge test (Figure S8), in which we intentionally left the full-cell at the end of charge for 5 h, before resuming the normal discharge. The open-circuit voltage dropped from 1.8 V to 1.3 V during the rest, and the resulting discharge capacity also decreased from 95 mAh g^{-1} in the previous cycle to 46 mAh g^{-1}, both indicative of a missing SEI in the dilute electrolyte. The interfacial instability is also confirmed by extended OEMS measurement for 15 cycles (Figure S9), in which sustained potential-dependent gas evolution for H_2, H_2S, and S_8 was noted. Although the material has been shown to be compatible with a 21 m WiS electrolyte,[25] the catalytic activity of TiS_2 towards HER may impose a great hurdle to its application in dilute electrolytes, in which water activity cannot be suppressed.

In order to tackle the challenge, the electrode-electrolyte interface and/or interphase has to be tailored. For example, we are currently evaluating the feasibility of surface coating by atomic layer deposition (ALD). Coating the active material by organic compounds, such as polymers, should also prevent the electrode from detrimental side-reactions while improving mechanical integrity. From an electrolyte perspective, film-forming additives may contribute to a robust SEI; lessons can be borrowed from the development of non-aqueous battery electrolytes.[41,42] Several other aspects that have not been discussed in detail from this work, such as prevention of current collector corrosion and impact of air on aqueous battery performance, should also be thoroughly resolved.

Lastly, the peculiarly higher potential profile of TiS_2 when cycled in aqueous electrolytes requires further clarification. Proton co-intercalation is possible and has been studied by other groups in a wider context.[27,43–46] It is worth noting that the investigated electrolyte is far from infinitely dilute in salt, meaning that the activity coefficient of Li^+ and H^+ cannot be taken as unity, hence the increased electrode potentials in more concentrated electrolytes based on the Nernst equation.[3,4,47,48] Future outlook includes employing an arsenal of complementary characterization techniques, such as *operando* X-ray diffraction, X-ray photoelectron spectroscopy, proton nuclear magnetic resonance spectroscopy, and advanced microscopies, together with computational modeling to deepen the fundamental understanding of the underlying chemistry.

Conclusion

In summary, we explored the compatibility of TiS_2 with dilute aqueous electrolytes in sustainable ALiBs. The assembled $LiMn_2O_4$||TiS_2 full-cells, based on a 2 m LiTFSI aqueous electrolyte, deliver a reversible discharge capacity of ca. 80 mAh g^{-1} in the first few cycles, at a current density of 50 mA g^{-1}. Afterwards, the performance gradually degrades as a result of increasing electrode-electrolyte side-reactions, since no stable SEI is formed. In this work, we observe a potential profile for TiS_2, when cycled in aqueous electrolytes, not only *ca.* 600 mV higher than when cycled in a non-aqueous electrolyte, but also significantly different in shape. Based on complementary OEMS measurements, potential-dependent H_2, H_2S, and elemental sulfur evolutions are observed and relate the TiS_2 potential

profile to several competing processes, such as 1) solvated water/hydronium cation (H_3O^+) intercalation/deintercalation, 2) partial TiS_2 exfoliation and 3) TiS_2-catalyzed water splitting in dilute aqueous electrolytes. Our work provides new perspectives to the understanding of electrode-electrolyte interface and interphase in aqueous Li-ion batteries using dilute electrolytes, which serve as building-blocks to design sustainable energy storage technologies either succeeding or complementing the existing battery chemistries on the market.

Experimental Section

Electrode preparation: $LiMn_2O_4$ (battery grade, SEDEMA) and TiS_2 (99.9%, Sigma Aldrich) were used without purification. A powder mixture containing 80 wt% of active material, 10 wt% of carbon SC65, and 10 wt% of polyvinylidene difluoride (PVdF) HSV900 were dissolved in *n*-methyl-2-pyrrolidone (NMP) and homogenized by a Polytron PT2500E turbo-mixer. Slurries were coated by doctor blade technique on either a piece of 316 L stainless steel foil (for $LiMn_2O_4$) or mesh (for TiS_2), with wet thicknesses of 400 μm and 120 μm, respectively.

Cell assembly and testing: All cells were assembled in an Ar-filled glovebox with both H_2O and O_2 content less than 0.1 ppm. TiS_2 coin-type half-cells were assembled using Li metal as the anode, two pieces of Whatman GF/A glassfiber as the separator, and 80 μL LP40 electrolyte. Coin-type aqueous full-cells were assembled anode-limited (2.5 : 1), using $LiMn_2O_4$ as the cathode (areal loading *ca.* 8.3 mg cm^{-2}), TiS_2 as the anode (areal loading ca. 5.9 mg cm^{-2}), two pieces of GF/A glassfiber as the separator, and 80 μL aqueous electrolyte comprising 2 m LiTFSI dissolved in Milli-Q water. Swagelok-type three-electrode aqueous cells were assembled by incorporating a commercial Ag/AgCl reference electrode (0.23 V vs. SHE). A current density of 50 mA g^{-1} was systematically applied for all cells (which roughly corresponds to 0.2 C), with a cycling window of 1.7–3.2 V for half-cells and 0.01–1.8 V for full-cells.

OEMS analysis: *Operando* gas analysis measurements were performed using an in-house designed setup reported in Ref. [33]. Volatile species at the headspace of the OEMS cell were intermittently sampled by a mass spectrometer (QME220, Pfeiffer) through a capillary. High-purity Ar (99.9999%, Air Liquide) was used as the carrier gas. Ion currents at different mass-to-charge (*m/z*) channels of 2, 32, 34, and 64 were measured and converted to gas evolution rates. The ion current at $m/z = 2$, which corresponds to H_2 evolution, has been calibrated by a calibration gas of 2000 ppm of H_2 in Ar.

Acknowledgements

The authors acknowledge the Swedish Energy Agency (Grant 50119-1), Knut and Alice Wallenberg (KAW) Foundation (Grant 2017.0204), Swedish Research Council (2016-04069), and Stiftelsen för Strategisk Forskning (SSF, FFL18-0269) for financial support and StandUp for Energy for base funding. Mr. Jackie T. Yik is acknowledged for proofreading.

Conflict of Interest

The authors declare no conflict of interest.

Data Availability Statement

The data that support the findings of this study are available from the corresponding author upon reasonable request.

Keywords: aqueous lithium-ion batteries · interfaces · layered compounds · mass spectrometry · water splitting

[1] W. Li, J. R. Dahn, D. S. Wainwright, *Science* **1994**, *264*, 1115–1118.
[2] E. Peled, S. Menkin, *J. Electrochem. Soc.* **2017**, *164*, A1703–A1719.
[3] L. Suo, O. Borodin, T. Gao, M. Olguin, J. Ho, X. Fan, C. Luo, C. Wang, K. Xu, *Science.* **2015**, *350*, 938–943.
[4] Y. Yamada, K. Usui, K. Sodeyama, S. Ko, Y. Tateyama, A. Yamada, *Nat. Energy* **2016**, *1*, 16129.
[5] J. Zhao, J. Zhang, W. Yang, B. Chen, Z. Zhao, H. Qiu, S. Dong, X. Zhou, G. Cui, L. Chen, *Nano Energy* **2019**, *57*, 625–634.
[6] X. Hou, T. P. Pollard, X. He, L. Du, X. Ju, W. Zhao, M. Li, J. Wang, E. Paillard, H. Lin, J. Sun, K. Xu, O. Borodin, M. Winter, J. Li, *Adv. Energy Mater.* **2022**, *12*, 2200401.
[7] L. Droguet, A. Grimaud, O. Fontaine, J. M. Tarascon, *Adv. Energy Mater.* **2020**, *10*, 2002440.
[8] J. Yue, J. Zhang, Y. Tong, M. Chen, L. Liu, L. Jiang, T. Lv, Y. sheng Hu, H. Li, X. Huang, L. Gu, G. Feng, K. Xu, L. Suo, L. Chen, *Nat. Chem.* **2021**, *13*, 1061–1069.
[9] J. Xie, Z. Liang, Y. C. Lu, *Nat. Mater.* **2020**, *19*, 1006–1011.
[10] D. Chao, W. Zhou, F. Xie, C. Ye, H. Li, M. Jaroniec, S. Z. Qiao, *Sci. Adv.* **2020**, *6*, eaba4098.
[11] M. S. Whittingham, *Chem. Rev.* **2004**, *104*, 4271–4301.
[12] M. S. Whittingham, *Science* **1976**, *192*, 1126–1127.
[13] X. Wang, C. Bommier, Z. Jian, Z. Li, R. S. Chandrabose, I. A. Rodríguez-Pérez, P. A. Greaney, X. Ji, *Angew. Chem. Int. Ed.* **2017**, *56*, 2909–2913; *Angew. Chem.* **2017**, *129*, 2955–2959.
[14] L. Zhang, D. Sun, J. Kang, H. T. Wang, S. H. Hsieh, W. F. Pong, H. A. Bechtel, J. Feng, L. W. Wang, E. J. Cairns, J. Guo, *Nano Lett.* **2018**, *18*, 4506–4515.
[15] H. Tao, M. Zhou, R. Wang, K. Wang, S. Cheng, K. Jiang, H. Tao, M. Zhou, R. Wang, K. Wang, S. Cheng, K. Jiang, *Adv. Sci.* **2018**, *5*, 1801021.
[16] L. Wang, J. Zou, S. Chen, G. Zhou, J. Bai, P. Gao, Y. Wang, X. Yu, J. Li, Y. S. Hu, H. Li, *Energy Storage Mater.* **2018**, *12*, 216–222.
[17] X. Sun, P. Bonnick, L. F. Nazar, *ACS Energy Lett.* **2016**, *1*, 297–301.
[18] L. Wang, M. Jiang, F. Liu, Q. Huang, L. Liu, L. Fu, Y. Wu, *Energy Fuels* **2020**, *34*, 11590–11596.
[19] R. Verrelli, A. Black, R. Dugas, D. Tchitchekova, A. Ponrouch, M. R. Palacin, *J. Electrochem. Soc.* **2020**, *167*, 070532.
[20] J. Han, A. Varzi, S. Passerini, *Angew. Chem. Int. Ed.* **2022**, *61*, e202115046.
[21] G. Li, D. Zhang, Q. Qiao, Y. Yu, D. Peterson, A. Zafar, R. Kumar, S. Curtarolo, F. Hunte, S. Shannon, Y. Zhu, W. Yang, L. Cao, *J. Am. Chem. Soc.* **2016**, *138*, 16632–16638.
[22] T. Das, S. Chakraborty, R. Ahuja, G. P. Das, *ChemPhysChem* **2019**, *20*, 608–617.
[23] C. Lin, X. Zhu, J. Feng, C. Wu, S. Hu, J. Peng, Y. Guo, L. Peng, J. Zhao, J. Huang, J. Yang, Y. Xie, *J. Am. Chem. Soc.* **2013**, *135*, 5144–5151.
[24] Q. Li, L. Shi, R. Wu, C. Lin, X. Bai, Y. Ouyang, B. A. Baraiya, P. K. Jha, J. Wang, *Phys. Chem. Chem. Phys.* **2019**, *21*, 17010–17017.
[25] W. Sun, L. Suo, F. Wang, N. Eidson, C. Yang, F. Han, Z. Ma, T. Gao, M. Zhu, C. Wang, *Electrochem. Commun.* **2017**, *82*, 71–74.
[26] E. Long, S. O'Brien, E. A. Lewis, E. Prestat, C. Downing, C. S. Cucinotta, S. Sanvito, S. J. Haigh, V. Nicolosi, *NPJ 2D Mater. Appl.* **2017**, *1*, 1–9.
[27] W. Li, K. Wang, S. Cheng, K. Jiang, W. Li, K. Wang, S. Cheng, K. Jiang, *Adv. Energy Mater.* **2019**, *9*, 1900993.
[28] D. Streich, C. Erk, A. Guéguen, P. Müller, F. F. Chesneau, E. J. Berg, *J. Phys. Chem. C* **2017**, *121*, 13481–13486.
[29] L. Zhang, C. Tsolakidou, S. Mariyappan, J. M. Tarascon, S. Trabesinger, *Energy Storage Mater.* **2021**, *42*, 12–21.
[30] T. Bartsch, F. Strauss, T. Hatsukade, A. Schiele, A. Y. Kim, P. Hartmann, J. Janek, T. Brezesinski, *ACS Energy Lett.* **2018**, *3*, 2539–2543.
[31] R. Jung, M. Metzger, D. Haering, S. Solchenbach, C. Marino, N. Tsiouvaras, C. Stinner, H. A. Gasteiger, *J. Electrochem. Soc.* **2016**, *163*, A1705–A1716.

[32] B. D. McCloskey, D. S. Bethune, R. M. Shelby, G. Girishkumar, A. C. Luntz, *J. Phys. Chem. Lett.* **2011**, *2*, 1161–1166.
[33] R. Lundström, E. J. Berg, *J. Power Sources* **2021**, *485*, 229347.
[34] L. Zhang, E. A. M. Gubler, C.-W. Tai, Ł. Kondracki, H. Sommer, P. Novák, M. El Kazzi, S. Trabesinger, *ACS Appl. Mater. Interfaces* **2022**, *14*, 13240–13249.
[35] J. R. Hall, M. H. Schoenfisch, *Anal. Chem.* **2018**, *90*, 5194–5200.
[36] A. A. Vostrikov, O. N. Fedyaeva, A. V. Shishkin, M. Y. Sokol, *J. Eng. Thermophys.* **2017**, *26*, 314–324.
[37] P. Biswal, S. Stalin, A. Kludze, S. Choudhury, L. A. Archer, *Nano Lett.* **2019**, *19*, 8191–8200.
[38] L. Lutz, W. Dachraoui, A. Demortière, L. R. Johnson, P. G. Bruce, A. Grimaud, J. M. Tarascon, *Nano Lett.* **2018**, *18*, 1280–1289.
[39] L. Zhang, J. M. Tarascon, M. T. Sougrati, G. Rousse, G. Chen, *J. Mater. Chem. A* **2015**, *3*, 16988–16997.
[40] M. Farooque, T. Z. Fahidy, *J. Electrochem. Soc.* **1978**, *125*, 544–546.
[41] K. Xu, *Chem. Rev.* **2004**, *104*, 4303–4417.
[42] K. Xu, *Chem. Rev.* **2014**, *114*, 11503–11618.
[43] S. Bi, Y. Zhang, S. Deng, Z. Tie, Z. Niu, *Angew. Chem. Int. Ed.* **2022**, *61*, e202200809.
[44] F. Wang, L. E. Blanc, Q. Li, A. Faraone, X. Ji, H. H. Chen-Mayer, R. L. Paul, J. A. Dura, E. Hu, K. Xu, L. F. Nazar, C. Wang, *Adv. Energy Mater.* **2021**, *11*, 2102016.
[45] L. Zhou, L. Liu, Z. Hao, Z. Yan, X. F. Yu, P. K. Chu, K. Zhang, J. Chen, *Matter* **2021**, *4*, 1252–1273.
[46] W. Sun, F. Wang, S. Hou, C. Yang, X. Fan, Z. Ma, T. Gao, F. Han, R. Hu, M. Zhu, C. Wang, *J. Am. Chem. Soc.* **2017**, *139*, 9775–9778.
[47] D. Degoulange, N. Dubouis, A. Grimaud, *J. Chem. Phys.* **2021**, *155*, 064701.
[48] M. McEldrew, Z. A. H. Goodwin, S. Bi, M. Z. Bazant, A. A. Kornyshev, *J. Chem. Phys.* **2020**, *152*, 234506.

Manuscript received: July 30, 2022
Revised manuscript received: September 16, 2022
Accepted manuscript online: September 20, 2022
Version of record online: October 7, 2022